Shell-model calculation of ^{100}Mo double-β decay

L. Coraggio,[1,2] N. Itaco,[1,2] G. De Gregorio,[1,2] A. Gargano,[2] R. Mancino,[1,2] and F. Nowacki[3,4]

[1]*Dipartimento di Matematica e Fisica, Università degli Studi della Campania "Luigi Vanvitelli", Viale Abramo Lincoln 5, I-81100 Caserta, Italy*

[2]*Istituto Nazionale di Fisica Nucleare, Complesso Universitario di Monte S. Angelo, Via Cintia, I-80126 Napoli, Italy*

[3]*Université de Strasbourg, IPHC, 23 rue du Loess 67037 Strasbourg, France*

[4]*CNRS, IPHC UMR 7178, 67037 Strasbourg, France*

(Received 24 September 2021; accepted 28 February 2022; published 10 March 2022)

For the first time, the calculation of the nuclear matrix element of the double-β decay of ^{100}Mo, with and without the emission of two neutrinos, is performed in the framework of the nuclear shell model. This task is accomplished starting from a realistic nucleon-nucleon potential, then the effective shell-model Hamiltonian and decay operators are derived within the many-body perturbation theory. The exotic features which characterize the structure of Mo isotopes—such as shape coexistence and triaxiality softness—push the shell-model computational problem beyond its present limits, making it necessary to truncate the model space. This has been done with the goal to preserve as much as possible the role of the rejected degrees of freedom in an effective approach that has been introduced and tested in previous studies. This procedure is grounded on the analysis of the effective single-particle energies of a large-scale shell-model Hamiltonian, that leads to a truncation of the number of the orbitals belonging to the model space. Then, the original Hamiltonian generates a new one by way of a unitary transformation onto the reduced model space, to retain effectively the role of the excluded single-particle orbitals. The predictivity of our calculation of the nuclear matrix element for the neutrinoless double-β decay of ^{100}Mo is supported by comparison with experiments of the calculated spectra, electromagnetic transition strengths, Gamow-Teller transition strengths, and the two-neutrino double-β nuclear matrix elements.

DOI: 10.1103/PhysRevC.105.034312

I. INTRODUCTION

Between the late 1990s and the early 2000s, the observation that solar and atmospheric neutrinos oscillate [1,2] has indicated that these elusive particles have nonzero mass, and has supported investigations to search for physics beyond the standard model [3,4]. This discovery has revived interest in the study of neutrinoless double-β decay ($0\nu\beta\beta$), a rare second-order electroweak process that, if occurring, would provide fundamental knowledge about the nature of the neutrino. In fact, such a decay would demonstrate that neutrinos are Majorana particles, namely they are their own antiparticles, and violate the conservation of lepton quantum number. Moreover, the measurement of the half-life of $0\nu\beta\beta$ decay would be a source of knowledge about the absolute scale of neutrino masses and their hierarchy, normal or inverted [5].

The standard mechanism that is considered in a $0\nu\beta\beta$ decay is the exchange of a light Majorana neutrino, and in such a framework the half-life is expressed as

$$\left[T^{0\nu}_{1/2}\right]^{-1} = G^{0\nu} g_A^4 |M^{0\nu}|^2 \left| \frac{\langle m_\nu \rangle}{m_e} \right|^2, \tag{1}$$

where $G^{0\nu}$ is the phase-space factor [6,7], $M^{0\nu}$ is the nuclear matrix element directly related to the wave functions of the parent and granddaughter nuclei, g_A is the axial coupling constant, m_e is the electron mass, and $\langle m_\nu \rangle = \sum_i (U_{ei})^2 m_i$ is the effective neutrino mass, as expressed in terms of the neutrino masses m_i and their mixing matrix elements U_{ei}.

The expression in (1) makes explicit the crucial role of the physics of nuclear structure, since the calculation of $M^{0\nu}$, which cannot be measured, provides the value of the neutrino effective mass in terms of the half-life $T^{0\nu}_{1/2}$ and of the nuclear structure factor $F_N = G^{0\nu}|M^{0\nu}|^2 g_A^4$. The value of $M^{0\nu}$ is also important to estimate the half-life that an experiment should measure in order to be sensitive to a particular value of the neutrino effective mass [8], by combining the nuclear structure factor, the neutrino mixing parameters [9], and present limits on $\langle m_\nu \rangle$ from current observations.

It is then highly desirable that the theory could provide reliable calculations of $M^{0\nu}$, namely that all uncertainties and truncations which characterize the application of a nuclear model are under control, leading eventually to an estimate of the theoretical error. This is currently within reach of *ab initio* calculations, but at present this approach has been pursued mainly for light nuclei [10–12] whereas the best candidates of experimental interest are located in the region of medium- and heavy-mass nuclei. The nuclear matrix element of $0\nu\beta\beta$ decay of ^{48}Ca, the lightest nuclide of experimental interest, has been also calculated using both an *ab initio* approach which combines the in-medium similarity renormalization group (IMSRG) with the generator coordinate method [13], and the coupled cluster method [14]. More recently, a

calculation of $M^{0\nu}$'s for the $0\nu\beta\beta$ decay of ^{48}Ca, ^{76}Ge, and ^{82}Se was performed in terms of the in-medium similarity renormalization group [15].

Presently, the study of nuclei that are the target of ongoing experiments cannot be performed within the *ab initio* framework, and the nuclear structure models which are mostly employed are the interacting boson model (IBM) [16], the quasiparticle random-phase approximation (QRPA) [17,18], energy density functional (EDF) methods [19,20], the covariant density functional theory [21,22], the generator-coordinate method (GCM) [23,24], and the shell model (SM) [25–30].

Among several candidates for the detection of $0\nu\beta\beta$ decay, ^{100}Mo is nowadays one of the most interesting ones. ^{100}Mo is characterized by one of the largest decay energies ($Q_{\beta\beta} = 3034.36 \pm 0.17$ keV) [31], which largely suppresses the γ background, and its natural abundance of 9.7% makes experiments that are targeted to this nuclide accessible with ton-scale detectors.

Experiments that are searching $0\nu\beta\beta$ decay of ^{100}Mo are AMoRE [32,33], NEMO 3 [34], CUPID-Mo [35,36], and in future the ton-scale CUPID (CUORE Upgrade with Particle IDentification) [37].

Recently, the CUPID-Mo experiment imposed a new limit on the half-life of $0\nu\beta\beta$ decay in ^{100}Mo of $T^{0\nu}_{1/2} > 1.5 \times 10^{24}$ yr [36].

Despite its encouraging features as a candidate for the detection of neutrinoless double-β decay, the structure of ^{100}Mo poses serious difficulties for a microscopic calculation of the β-decay properties of this nuclide and consequently of its $0\nu\beta\beta$-decay nuclear matrix element. Since the 1970s there is experimental evidence for a rotational behavior of neutron-rich Mo isotopes [38], and many nuclear structure studies have been carried out to study their transition from spherical to deformed shapes, as well as to search for shape coexistence and triaxiality [39–43].

Collective models are then better endowed for a satisfactory description of heavy-mass molybdenum isotopes than microscopic ones, and there are few calculations of ^{100}Mo spectroscopic properties within the nuclear shell model [44,45]. Calculation of β-decay properties of ^{100}Mo and estimates of its $0\nu\beta\beta$-decay nuclear matrix element have been carried out within the framework of EDF [21,46], IBM [16,47], and extensively with QRPA and proton-neutron QRPA (pnQRPA) [48–52].

In the present work, for the first time, the study of the double-β decay of ^{100}Mo is approached from the point of view of the realistic shell model (RSM) [53], namely the effective SM Hamiltonian $H_{\rm eff}$ and decay operators are consistently derived starting from a realistic nucleon-nucleon (NN) potential V^{NN}.

The starting point is the high-precision CD-Bonn NN potential [54], whose repulsive high-momentum components are renormalized using the $V_{\text{low-}k}$ procedure [55]. The low-momentum $V_{\text{low-}k}$ is amenable to a perturbative expansion of the shell-model effective Hamiltonian [56–59] and decay operators [60,61], so that single-particle (SP) energies, two-body matrix elements of the residual interaction (TBMEs), matrix elements of effective electromagnetic transitions and Gamow-Teller (GT) decay operators, as well as two-body matrix elements of the effective $0\nu\beta\beta$-decay operator are derived in terms of a microscopic approach, without adjusting SM parameters to reproduce data. This approach was recently employed first to study two-neutrino double-β ($2\nu\beta\beta$) decay of ^{48}Ca, ^{76}Ge, ^{82}Se, ^{130}Te, and ^{136}Xe [62,63], and then to calculate $M^{0\nu}$'s of the same nuclides for their $0\nu\beta\beta$ decay [64].

The model space we choose to calculate the nuclear wave functions of ^{100}Mo and ^{100}Ru, which are the main characters of the decay process we investigate in this work, is spanned by four proton orbitals $0f_{5/2}, 1p_{3/2}, 1p_{1/2}, 0g_{9/2}$ and five neutron orbitals $0g_{7/2}, 1d_{5/2}, 1d_{3/2}, 2s_{1/2}, 0h_{11/2}$ outside ^{78}Ni core, which is characterized by the $Z = 28, N = 50$ shell closures. This means that the structure of ^{100}Mo should be described in terms of 14 and 8 valence protons and neutrons, respectively, interacting in such a large model space, while ^{100}Ru is characterized by 16 and 6 valence protons and neutrons.

Note that such a model space may not be large enough to account for the ground-state deformation of nuclei around $A \approx 100$ such as ^{100}Zr [65], and that perhaps $Z, N = 50$ cross-shell excitations should be explicitly included to reproduce the large observed $B(E2; 2^+_1 \to 0^+_1)$ values [66]. However, as we will see in Sec. III, this choice of the model space does not seem to affect the overall comparison between the experimental and our calculated $B(E2)$'s, for both ^{100}Mo and ^{100}Ru.

The computational problem has a high degree of difficulty, being at the limit of actual capabilities and burdensome to handle. We have employed a procedure that aims to reduce the computational complexity of large-scale shell-model calculations, by preserving effectively the role of the rejected degrees of freedom. First, the truncation is driven by the analysis of the effective SP energies (ESPE) of the original Hamiltonian, in order to locate the relevant degrees of freedom to describe $A = 100$ Mo, Tc, and Ru isotopes, namely the single-particle orbitals that will constitute a smaller and manageable model space. As a second step, we perform a unitary transformation of the original Hamiltonian, defined in the model space that is made up respectively by four and five proton and neutron orbitals (labeled as [4 5]), onto the truncated model space. This transformation generates a new shell-model Hamiltonian that, even if defined within a smaller number of configurations, retains effectively the role of the excluded SP orbitals.

This double-step procedure, that is, to derive a first $H_{\rm eff}$ in a large space and then from this a new one in a smaller space, was introduced in Refs. [66,67] for nuclei in the mass region $A \approx 100$ outside the ^{88}Sr core, and successfully applied also for Mo isotopes up to $A = 98$ [66].

In the following section we outline first the derivation of $H_{\rm eff}$ and SM effective decay operators by way of the many-body perturbation theory. Then, we sketch out some details about the double-step procedure to derive a new $H_{\rm eff}$ in a smaller space, and show an example aimed to support its validity. In Sec. III we report the calculated low-energy spectroscopic properties of the nuclei involved in the double-β decay process under investigation, the parent and granddaughter nuclei ^{100}Mo, Ru, as well as the calculated GT-strength

distributions and $M^{2\nu}$'s, and compare them with available data. In the same section we report the results of the calculation of $M^{0\nu}$ for ^{100}Mo, together with an analysis of the angular momentum-parity matrix-element distributions, and a comparison with the results obtained with other nuclear structure models. Finally, the last section is devoted to a summary of the present work and an outlook of our future developments.

II. THEORETICAL FRAMEWORK

A. The effective SM Hamiltonian

The starting point of our calculation is the high-precision CD-Bonn NN potential [54], whose repulsive high-momentum components—that prevent a perturbative approach to the many-body problem—are renormalized by way of the $V_{\text{low-}k}$ approach [53,55].

This unitary transformation provides a smooth potential that preserves the values of all NN observables calculated with the CD-Bonn potential, as well as the contribution of the short-range correlations (SRC). The latter account for the action of a two-body decay operator on an unperturbed (uncorrelated) wave function, which is employed to derive the SM effective $0\nu\beta\beta$ operator; this is different from applying the same operator on the real (correlated) nuclear wave function. The details about the treatment of SRC consistently with the $V_{\text{low-}k}$ transformation are reported in Refs. [30,64,68].

The $V_{\text{low-}k}$ matrix elements are then employed as interaction vertices of the perturbative expansion of H_{eff}, and detailed surveys about this topic can be found in Refs. [57,59,61]. Here, we sketch briefly the procedure that has been followed to derive H_{eff} and SM effective decay operators.

We begin by considering the full nuclear Hamiltonian for A interacting nucleons H, which, within the nuclear shell model, is broken up as a sum of a one-body term H_0, whose eigenvectors set up the SM basis, and a residual interaction H_1, by way of harmonic-oscillator (HO) one-body potential U:

$$\begin{aligned} H &= T + V_{\text{low-}k} = (T+U) + (V_{\text{low-}k} - U) \\ &= H_0 + H_1. \end{aligned} \tag{2}$$

Since this Hamiltonian cannot be diagonalized for a many-body system in an infinite basis of eigenvectors of H_0, we derive an effective Hamiltonian, which operates in a truncated model space that, in order to obtain a satisfactory description of ^{100}Mo, is spanned by four proton orbitals ($0f_{5/2}$, $1p_{3/2}$, $1p_{1/2}$, $0g_{9/2}$) and five neutron orbitals ($0g_{7/2}$, $1d_{5/2}$, $1d_{3/2}$, $2s_{1/2}$, $0h_{11/2}$) outside the ^{78}Ni core. From now on, we denote this model space as [4 5].

To this end, we perform a similarity transformation which provides, within the full Hilbert space of the configurations, a decoupling of the model space P, where the valence nucleons are constrained, from its complement $Q = 1 - P$.

This may be obtained within the time-dependent perturbation theory, namely we derive H_{eff} through the Kuo-Lee-Ratcliff folded-diagram expansion in terms of the $\hat{Q}$ box vertex function [57,59,69]:

$$H_1^{\text{eff}}(\omega) = \hat{Q}(\epsilon_0) - PH_1Q\frac{1}{\epsilon_0 - QHQ}\omega H_1^{\text{eff}}(\omega), \tag{3}$$

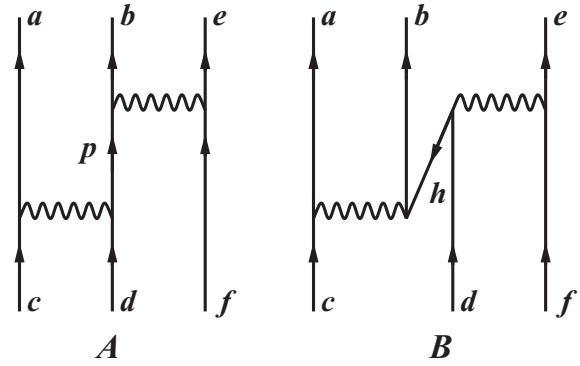

FIG. 1. Second-order three-body diagrams. The sum over the intermediate lines runs over particle and hole states outside the model space. For each topology A and B, only one of the diagrams which correspond to the permutations of the external lines is reported.

where ω is the wave operator decoupling the P and Q subspaces, and ϵ_0 is the eigenvalue of the unperturbed degenerate Hamiltonian H_0.

The $\hat{Q}$ box is defined as

$$\hat{Q}(\epsilon) = PH_1P + PH_1Q\frac{1}{\epsilon - QHQ}QH_1P, \tag{4}$$

and ϵ is an energy parameter called "starting energy."

An exact calculation of the $\hat{Q}$ box is computationally prohibitive, so the term $1/(\epsilon - QHQ)$ is expanded as a power series

$$\frac{1}{\epsilon - QHQ} = \sum_{n=0}^{\infty}\frac{1}{\epsilon - QH_0Q}\left(\frac{QH_1Q}{\epsilon - QH_0Q}\right)^n; \tag{5}$$

namely, we perform an expansion of the $\hat{Q}$ box up to the third order in perturbation theory [61].

Then, the $\hat{Q}$ box is the building block to solve the nonlinear matrix equation (3) to derive H_{eff} through iterative techniques such as the Kuo-Krenciglowa and Lee-Suzuki ones [70,71], or graphical noniterative methods [72].

This theoretical framework has been well established for systems with one- and two-valence nucleon systems, but, because of the choice of the model space, the nuclei that are involved in the decay process under investigation—^{100}Mo, Tc, Ru—are characterized by 22 valence nucleons. Then, one should derive a many-body H_{eff} which depends on this number of valence particles, and introduce a formalism that may become very difficult to manage. A minimal choice is to include in the calculation of the $\hat{Q}$ box at least contributions from three-body diagrams, which account for the interaction via the two-body force of the valence nucleons with configurations outside the model space (see Fig. 1).

Since we employ the SM code ANTOINE to calculate the spectra and double β-decay nuclear matrix elements [73], a diagonalization of a three-body H_{eff} cannot be performed and we derive a density-dependent two-body term from the three-body contribution arising at second order in perturbation theory. The details of such an approach, as well as a discussion about the role of such contributions to the eigenvalues of the SM Hamiltonian, can be found in Refs. [61,74].

TABLE I. Theoretical proton and neutron SP energy spacings (in MeV) from $H_{\rm eff}^{[45]}$.

Proton orbitals	ϵ_p	Neutron orbitals	ϵ_n
$0f_{5/2}$	0.0	$0g_{7/2}$	2.8
$1p_{3/2}$	1.6	$1d_{5/2}$	0.4
$1p_{1/2}$	2.1	$1d_{3/2}$	1.1
$0g_{9/2}$	4.3	$2s_{1/2}$	0.0
		$0h_{11/2}$	3.2

In the Introduction we pointed out that the current limits of the available SM codes prevent the calculation of the nuclear matrix elements of double-β decay within the [4 5] model space. In order to overcome this computational difficulty, we perform a truncation of the number of SP orbitals following a method we introduced in Ref. [67], and whose details may be found in Ref. [66].

We now sketch the main steps of this procedure.

First, we study the evolution of the proton and/or neutron ESPE as a function of the valence nucleons, that may justify the exclusion of one or more SP levels from the original model space (in our case [4 5]). Since ^{100}Mo is described in terms of 14 valence protons and 8 valence neutrons with respect to ^{78}Ni, this means that a truncation may be applied only to the number of the neutron orbitals.

In Table I we report the SP energy spacings calculated using the effective Hamiltonian $H_{\rm eff}^{[45]}$, which is defined within the model space [4 5], and in Fig. 2 we show the behavior of the neutron ESPE of the Mo isotopes. From the inspection of the table and the figure, we observe that there is an energy gap separating the $1d_{5/2}$, $1d_{3/2}$, $2s_{1/2}$ neutron orbitals from the $0g_{7/2}$, $0h_{11/2}$ ones, which enlarges by increasing the number of valence neutrons.

Therefore, we deem reasonable the possibility to exclude both $0g_{7/2}$ and $0h_{11/2}$ neutron orbitals, and deal with a smaller model space that should still provide the relevant features of the physics of the nuclei under investigation, namely the parent and granddaughter nuclei ^{100}Mo, Ru. However,

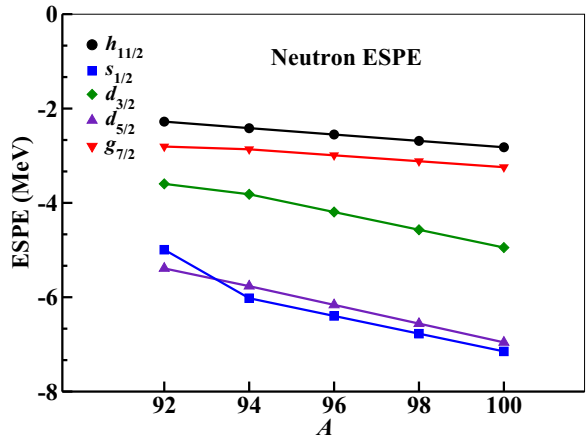

FIG. 2. Neutron effective single-particle energies of Mo isotopes calculated with $H_{\rm eff}^{[45]}$.

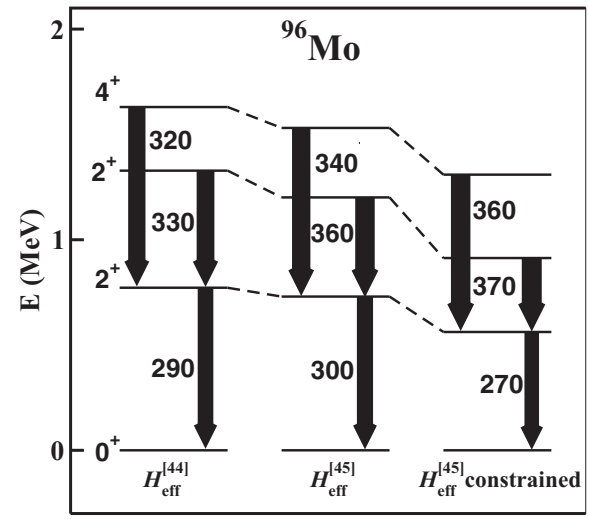

FIG. 3. Low-energy spectrum of ^{96}Mo, calculated with $H_{\rm eff}^{[45]}$, $H_{\rm eff}^{[44]}$, and constraining $H_{\rm eff}^{[45]}$ in the [4 4] model space. Also reported are the values of the significant $B(E2)$ transition rates in $e^2{\rm fm}^4$.

to calculate the nuclear matrix element for the two-neutrino double-β decay $M^{2\nu}$ of ^{100}Mo we need to retain at least the neutron $0g_{7/2}$ orbital in the model space, otherwise the selection rules of the GT operator would forbid such a decay because of the choice of the proton model subspace.

On these grounds, we derive a new effective Hamiltonian $H_{\rm eff}^{[44]}$, defined within a model space spanned by the $0f_{5/2}$, $1p_{3/2}$, $1p_{1/2}$, $0g_{9/2}$ proton and $0g_{7/2}$, $1d_{5/2}$, $1d_{3/2}$, $2s_{1/2}$ neutron orbitals, by way of a unitary transformation of $H_{\rm eff}^{[45]}$ (see details in Ref. [66]). We label this smaller model space [4 4] and in Fig. 3 we report the energy spectrum of ^{96}Mo, that is calculated employing $H_{\rm eff}^{[45]}$ and $H_{\rm eff}^{[44]}$, and also constraining the action of $H_{\rm eff}^{[45]}$ in the [4 4] model space.

From the inspection of Fig. 3, it can be noted that $H_{\rm eff}^{[44]}$ is able to provide a better agreement with the energy spectrum obtained through the "mother Hamiltonian" $H^{[45]}$ than the results provided by constraining the diagonalization of the latter Hamiltonian to model space [4 4]. It is also worth pointing out that the values of the $B(E2)$ transition rates, that are calculated with $H_{\rm eff}^{[45]}$ and $H_{\rm eff}^{[44]}$, are very close.

The above results evidence the adequacy of the truncation scheme we have adopted, and the diagonalization of the SM Hamiltonian for ^{100}Mo and ^{100}Ru has been performed by way of $H_{\rm eff}^{[44]}$.

The TBMEs of $H_{\rm eff}^{[44]}$, that have been calculated also including three-body correlations to account for the number of valence nucleons characterizing ^{100}Mo, can be found in the Supplemental Material [75].

B. Effective shell-model decay operators

We are interested not only in calculating energies, but also the matrix elements of decay operators Θ which are connected to measurable quantities such as $B(E2)$ strengths, and the nuclear matrix element of the $2\nu\beta\beta$ decay $M^{2\nu}$, as well as the $0\nu\beta\beta$ decay matrix element $M^{0\nu}$.

Since the diagonalization of the $H_{\rm eff}$ does not provide the true wave functions, but their projections onto the chosen model space P, we need to renormalize any decay operator Θ to take into account the neglected degrees of freedom corresponding to the Q space.

The derivation of SM effective operators within a perturbative approach dates back to the earliest attempts to employ realistic potentials for SM calculations [60,76–80], and we follow the procedure that has been introduced by Suzuki and Okamoto in Ref. [58]. This allows a calculation of decay operators $\Theta_{\rm eff}$ which is consistent with the one we carry out of $H_{\rm eff}$, and that is based on perturbative expansion of a vertex function $\hat{\Theta}$ box, analogously with the derivation of $H_{\rm eff}$ in terms of the $\hat{Q}$ box (see Sec. II A). The procedure has been reported in detail in Ref. [61], and in the following we only report the main building blocks.

The starting point is the perturbative calculation of the two energy-dependent vertex functions

$$\hat{\Theta}(\epsilon) = P\Theta P + P\Theta Q \frac{1}{\epsilon - QHQ} QH_1 P,$$

$$\hat{\Theta}(\epsilon_1;\epsilon_2) = PH_1 Q \frac{1}{\epsilon_1 - QHQ} Q\Theta Q \frac{1}{\epsilon_2 - QHQ} QH_1 P,$$

and of their derivatives calculated in $\epsilon = \epsilon_0$, ϵ_0 being the eigenvalue of the degenerate unperturbed Hamiltonian H_0:

$$\hat{\Theta}_m = \frac{1}{m!} \frac{d^m \hat{\Theta}(\epsilon)}{d\epsilon^m}\bigg|_{\epsilon=\epsilon_0},$$

$$\hat{\Theta}_{mn} = \frac{1}{m!n!} \frac{d^m}{d\epsilon_1^m} \frac{d^n}{d\epsilon_2^n} \hat{\Theta}(\epsilon_1;\epsilon_2)\bigg|_{\epsilon_1=\epsilon_0,\epsilon_2=\epsilon_0}.$$

Then, a series of operators χ_n is calculated:

$$\chi_0 = (\hat{\Theta}_0 + \text{H.c.}) + \hat{\Theta}_{00}, \tag{6}$$

$$\chi_1 = (\hat{\Theta}_1 \hat{Q} + \text{H.c.}) + (\hat{\Theta}_{01} \hat{Q} + \text{H.c.}),$$

$$\chi_2 = (\hat{\Theta}_1 \hat{Q}_1 \hat{Q} + \text{H.c.}) + (\hat{\Theta}_2 \hat{Q}\hat{Q} + \text{H.c.}) + (\hat{\Theta}_{02} \hat{Q}\hat{Q} + \text{H.c.}) + \hat{Q}\hat{\Theta}_{11}\hat{Q}, \tag{7}$$

$$\vdots$$

that allows us to write $\Theta_{\rm eff}$ in the following form:

$$\Theta_{\rm eff} = H_{\rm eff} \hat{Q}^{-1} (\chi_0 + \chi_1 + \chi_2 + \cdots). \tag{8}$$

In this work we arrest the χ_n series at $n = 2$, and the $\hat{\Theta}$ function is expanded up to third order in perturbation theory.

The issue of the convergence of the χ_n series and of the perturbative expansion of the $\hat{\Theta}$ box has been treated in Refs. [63,64,81], and in Fig. 4 are given all the diagrams up to second order appearing in the $\hat{\Theta}(\epsilon_0)$ expansion for a one-body operator Θ.

In the present work, the decay operators Θ are the one-body electric-quadrupole transition $E2$ $q_{p,n} r^2 Y^2_m(\hat{r})$—the charge $q_{p,n}$ being e for protons and 0 for neutrons—and GT $\vec{\sigma}\tau^{\pm}$ operators, as well as the two-body transition operator for the $0\nu\beta\beta$ decay [see Eqs. (13)–(15) in the following subsection].

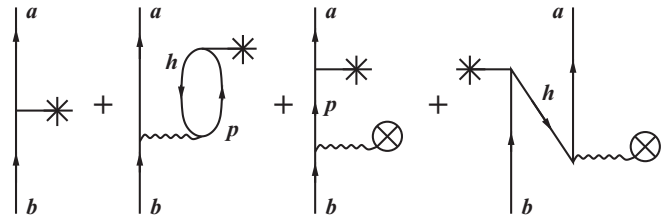

FIG. 4. One-body second-order diagrams included in the perturbative expansion of $\hat{\Theta}(\epsilon_0)$. The asterisk indicates the bare operator Θ, the wavy lines denote the two-body NN interaction, and the circle with a cross inside accounts for the $(V\text{-}U)$-insertion contribution (see Ref. [61]).

C. The $2\nu\beta\beta$- and $0\nu\beta\beta$-decay operators

This section is devoted to outlining the structure of $2\nu\beta\beta$- and $0\nu\beta\beta$-decay operators.

It is worth pointing out that these two nuclear-decay mechanisms differ in the characteristic value of the momentum transfer, which for $2\nu\beta\beta$ decay is few MeV, at variance with the order of hundreds of MeV in $0\nu\beta\beta$ decay. This difference, as we will see in the following, affects the procedure to be followed to calculate $M^{2\nu}$ and $M^{0\nu}$.

As is well known, $2\nu\beta\beta$ decays are the occurrence of two single-β decay transitions inside a nucleus, and the expressions of the GT and Fermi components of their nuclear matrix elements $M^{2\nu}$ are the following:

$$M^{2\nu}_{\rm GT} = \sum_n \frac{\langle 0^+_f || (\vec{\sigma}\tau^-)_{\mathcal{I}} || 1^+_n \rangle \langle 1^+_n || (\vec{\sigma}\tau^-)_{\mathcal{I}} || 0^+_i \rangle}{E_n + E_0}, \tag{9}$$

$$M^{2\nu}_{F} = \sum_n \frac{\langle 0^+_f || (\tau^-)_{\mathcal{I}} || 0^+_n \rangle \langle 0^+_n || (\tau^-)_{\mathcal{I}} || 0^+_i \rangle}{E_n + E_0}, \tag{10}$$

where the subscript $\mathcal{I}$ indicates we are employing the matrix elements of either the bare or the effective one-body GT and F operators.

In these equations, E_n is the excitation energy of the $J^\pi = 0^+_n, 1^+_n$ intermediate state, and $E_0 = \frac{1}{2} Q_{\beta\beta}(0^+) + \Delta M$, where $Q_{\beta\beta}(0^+)$ and ΔM are the Q value of the transition and the mass difference of the parent and daughter nuclear states, respectively. The index n runs over all possible intermediate states induced by the given transition operator. It should be pointed out that the Fermi component plays a marginal role [82,83] and in most calculations is neglected altogether.

The most efficient way to obtain $M^{2\nu}$, by including a number of intermediate states that is sufficient to provide the needed accuracy for its calculation, is the Lanczos strength-function method [73], which we have adopted for our calculations.

The evaluation of $M^{2\nu}$ could be also carried out employing the so-called closure approximation, commonly adopted to study $0\nu\beta\beta$-decay NMEs [82]. On these grounds, within such an approximation the energies of the intermediate states, E_n, appearing in Eqs. (9) and (10), may be replaced by an average value $E_n + E_0 \to \langle E \rangle$, that allows one to avoid to explicitly calculate the intermediate $J^\pi = 1^+_n$ states, but then the two one-body transition operators become a two-body operator.

Actually, the closure approximation is a valuable tool to evaluate $M^{0\nu}$, since in the $0\nu\beta\beta$ decay the neutrino's momentum is about one order of magnitude larger than the average excitation energy of the intermediate states. This allows us to neglect, within this process, the intermediate-state-dependent energies from the energy denominator appearing in the neutrino potential, as we will see in a while. In contrast, the closure approximation is unsatisfactory when used to calculate $M^{2\nu}$, because, as mentioned before, the momentum transfer in the $2\nu\beta\beta$ process is much smaller.

Once the theoretical value on $M^{2\nu}$ has been calculated, it can be then compared with the experimental counterpart, which is extracted from the observed half-life $T^{2\nu}_{1/2}$,

$$\left[T^{2\nu}_{1/2}\right]^{-1} = G^{2\nu}\left|M^{2\nu}_{\rm GT}\right|^2, \tag{11}$$

$G^{2\nu}$ being the $2\nu\beta\beta$-decay phase-space (or kinematic) factor [6,7].

We now turn our attention to the bare $0\nu\beta\beta$ operator, for the light-neutrino-exchange channel [84].

The formal expression of $M^{0\nu}_\alpha$, where α stands for Fermi (F), Gamow-Teller (GT), or tensor (T) decay channels, is written in terms of the one-body transition-density matrix elements between the daughter and parent nuclei (granddaughter and daughter nuclei) $\langle k|a^\dagger_{p'}a_{n'}|i\rangle$ ($\langle f|a^\dagger_p a_n|k\rangle$). The subscripts p and n denote proton and neutron states, and i, k, f refer to the parent, daughter, and granddaughter nuclei, respectively.

The nuclear matrix element $M^{0\nu}_\alpha$ is formulated as [25,85]

$$\begin{aligned} M^{0\nu}_\alpha &= \sum_{k\mathcal{J}}\sum_{j_p j_{p'} j_n j_{n'}} (-1)^{j_n+j_{n'}+\mathcal{J}}\hat{\mathcal{J}}\begin{Bmatrix} j_p & j_n & J_\kappa \\ j_{n'} & j_{p'} & \mathcal{J}\end{Bmatrix} \\ &\quad\times\langle j_p j_{p'};\mathcal{J}||\Theta^k_\alpha||j_n j_{n'};\mathcal{J}\rangle \\ &\quad\times\langle k||[a^\dagger_p\otimes\tilde{a}_n]_{J_k}||i\rangle\langle k||[a^\dagger_{n'}\otimes\tilde{a}_{p'}]_{J_k}||f\rangle^* \\ &= \sum_k\sum_{j_p j_{p'} j_n j_{n'}}\langle f|a^\dagger_p a_n|k\rangle\langle k|a^\dagger_{p'}a_{n'}|i\rangle \\ &\quad\times\langle j_p j_{p'}|\Theta^k_\alpha|j_n j_{n'}\rangle, \end{aligned} \tag{12}$$

where the tilde denotes a time-conjugated state, $\tilde{a}_{jm} = (-1)^{j+m}a_{j-m}$, and the Θ^k_α are two-body operators.

The expression of the operators Θ^k_α is [84]

$$\Theta^k_{\rm GT} = \left[\tau^-_1\tau^-_2(\vec{\sigma}_1\cdot\vec{\sigma}_2)H^k_{\rm GT}(r)\right]_{\mathcal{I}}, \tag{13}$$

$$\Theta^k_F = \left[\tau^-_1\tau^-_2 H^k_F(r)\right]_{\mathcal{I}}, \tag{14}$$

$$\Theta^k_T = \left[\tau^-_1\tau^-_2\{3(\vec{\sigma}_1\cdot\hat{r})(\vec{\sigma}_1\cdot\hat{r})-\vec{\sigma}_1\cdot\vec{\sigma}_2\}H^k_{\rm T}(r)\right]_{\mathcal{I}}, \tag{15}$$

where H_α are the neutrino potentials and are defined as

$$H^k_\alpha(r) = \frac{2R}{\pi}\int_0^\infty \frac{j_{n_\alpha}(qr)h_\alpha(q^2)q\,dq}{q+E_k-(E_i+E_f)/2}, \tag{16}$$

and, again, the subscript $\mathcal{I}$ labels the application of either the bare or the effective two-body decay operators.

In Eq. (16), $R = 1.2A^{1/3}$ fm, $j_{n_\alpha}(qr)$ is the spherical Bessel function, $n_\alpha = 0$ for Fermi and Gamow-Teller components, while $n_\alpha = 2$ for the tensor component. In the following, we also present the explicit expressions of neutrino form functions, $h_\alpha(q)$, for light-neutrino exchange [84]:

$$\begin{aligned} h_F(q^2) &= g^2_V(q^2), \\ h_{\rm GT}(q^2) &= \frac{g^2_A(q^2)}{g^2_A}\left[1-\frac{2}{3}\frac{q^2}{q^2+m^2_\pi}+\frac{1}{3}\left(\frac{q^2}{q^2+m^2_\pi}\right)^2\right] \\ &\quad+\frac{2}{3}\frac{g^2_M(q^2)}{g^2_A}\frac{q^2}{4m^2_p}, \\ h_T(q^2) &= \frac{g^2_A(q^2)}{g^2_A}\left[\frac{2}{3}\frac{q^2}{q^2+m^2_\pi}-\frac{1}{3}\left(\frac{q^2}{q^2+m^2_\pi}\right)^2\right] \\ &\quad+\frac{1}{3}\frac{g^2_M(q^2)}{g^2_A}\frac{q^2}{4m^2_p}, \end{aligned} \tag{17}$$

In the present work, we use the dipole approximation for the vector, $g_V(q^2)$, axial-vector, $g_A(q^2)$, and weak-magnetism, $g_M(q^2)$, form factors:

$$\begin{aligned} g_V(q^2) &= \frac{g_V}{\left(1+q^2/\Lambda^2_V\right)^2}, \\ g_M(q^2) &= (\mu_p-\mu_n)g_V(q^2), \\ g_A(q^2) &= \frac{g_A}{\left(1+q^2/\Lambda^2_A\right)^2}, \end{aligned} \tag{18}$$

where $g_V = 1$, $g_A \equiv g^{\rm free}_A = 1.2723$, $(\mu_p-\mu_n) = 4.7$, and the cutoff parameters are $\Lambda_V = 850$ MeV and $\Lambda_A = 1086$ MeV.

Then, the total nuclear matrix element $M^{0\nu}$ is written as

$$M^{0\nu} = M^{0\nu}_{\rm GT} - \frac{g^2_V}{g^2_A}M^{0\nu}_F + M^{0\nu}_T. \tag{19}$$

The expression in Eq. (12) cannot be easily calculated within the nuclear shell model because of the computational complexity of calculating a large number of intermediate states (the Lanczos strength-function method [73] can be applied only for the single-β-decay process). Therefore, most SM calculations resort to the closure approximation, which is based on the observation that the relative momentum q of the neutrino, appearing in the propagator of Eq. (16), is of the order of 100–200 MeV [84], and the excitation energies of the nuclei involved in the transition are of the order of 10 MeV [25]. On these grounds, the energies of the intermediate states appearing in Eq. (16) may be replaced by an average value $E_k-(E_i+E_f)/2 \to \langle E\rangle$, that leads to a simpler form of both Eqs. (12) and (16). Consequently, $M^{0\nu}_\alpha$ can be rewritten in terms of the two-body transition-density matrix elements $\langle f|a^\dagger_p a_n a^\dagger_{p'}a_{n'}|i\rangle$ as

$$\begin{aligned} M^{0\nu}_\alpha &= \sum_{j_n j_{n'} j_p j_{p'}}\langle f|a^\dagger_p a_n a^\dagger_{p'}a_{n'}|i\rangle \\ &\quad\times\langle j_p j_{p'}\mid\tau^-_1\tau^-_2\Theta_\alpha\mid j_n j_{n'}\rangle, \end{aligned} \tag{20}$$

and the neutrino potentials become

$$H_\alpha(r) = \frac{2R}{\pi}\int_0^\infty \frac{j_{n_\alpha}(qr)h_\alpha(q^2)q\,dq}{q+\langle E\rangle}. \tag{21}$$

As in most SM calculations, we adopt the closure approximation to define the Θ operators given in Eqs. (13)–(15), and

take the average energy $\langle E\rangle = 11.2$ MeV from the evaluation of Ref. [48]. Regarding the soundness of the closure approximation to evaluate $M^{0\nu}$, we should point out that in Ref. [25] the authors performed SM calculations of ^{48}Ca $0\nu\beta\beta$ decay both within and beyond the closure approximation, and found that in the second case the results are $\approx$10% larger.

As mentioned in Sec. II A, one needs to consider short-range correlations when computing the radial matrix elements of the neutrino potentials $\langle\psi_{nl}(r)|H_\alpha|\psi_{n'l'}(r)\rangle$.

SRC account for the physics that is missing in all models that expand nuclear wave functions in terms of a truncated noncorrelated SP basis [86,87]. This is related to the highly repulsive nature of the short-range two-nucleon interaction, and in order to carry out our SM calculation, that is based on effective operators derived from a realistic potential, we perform a consistent regularization both of the two-nucleon potential, V^{NN}, and the $0\nu\beta\beta$-decay operator [68].

The $V_{\text{low-}k}$ procedure [55] renormalizes the repulsive high-momentum components of the V^{NN} potential through a unitary transformation Ω. The latter is an operator which decouples the full momentum space of the two-nucleon Hamiltonian, H^{NN}, into two subspaces; the first one is associated with the relative-momentum configurations below a cutoff Λ and is specified by a projector operator P; the second one is defined in terms of its complement $Q = \mathbf{1} - P$ [68]. As unitary transformation, Ω preserves the physics of the original potential for the two-nucleon system; namely, the calculated values of all NN observables are the same as those reproduced by solving the Schrödinger equation for two nucleons interacting via V^{NN}.

In order to benefit from this procedure, we calculate the two-body $0\nu\beta\beta$ operator, Θ, in the momentum space. Then, Θ is renormalized using Ω, to provide consistency with the V^{NN} potential, whose high-momentum (short range) components are dumped by the introduction of the cutoff Λ. The new decay operator is defined as $\Theta_{\text{low-}k} \equiv P\Omega\Theta\Omega^{-1}P$ for relative momenta $k < \Lambda$, and is set to zero for $k > \Lambda$, and its matrix elements are employed as vertices in the perturbative expansion of the $\hat{\Theta}$ box.

The magnitude of the overall effect of this renormalization procedure is comparable to using the SRC modeled by the unitary correlation operator method [88], that is a lighter softening of $M^{0\nu}$ with respect to the one provided by Jastrow type SRC [68].

III. RESULTS

In this section we present the results of our SM calculations. First, we compare theoretical and experimental low-energy spectroscopic properties of the parent and granddaughter nuclei ^{100}Mo and ^{100}Ru, respectively. We show also the results of the GT$^-$ strength distribution and the calculated NMEs of the $2\nu\beta\beta$ decay for ^{100}Mo and compare them with the available data.

Then, we calculate the nuclear matrix element of the $0\nu\beta\beta$ decay and study the convergence behavior of the effective SM operator we have derived consistently with H_{eff}. We also discuss the effects of three-valence-nucleon diagrams which correct the Pauli-principle violation introduced in systems with more than two valence nucleons [80].

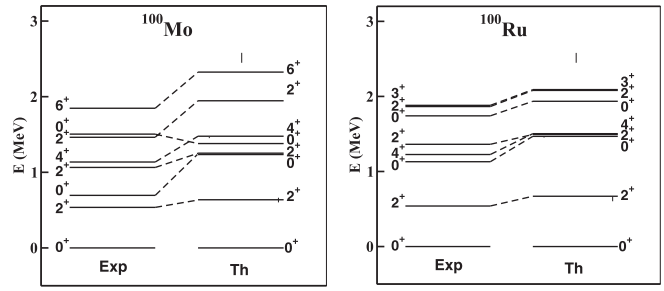

FIG. 5. Experimental and calculated spectra of ^{100}Mo and ^{100}Ru up to 2 MeV excitation energy.

As already mentioned, all the calculations are performed employing theoretical SP energies and TBMEs obtained from the effective Hamiltonian $H_{\text{eff}}^{[44]}$, whose model space is defined by $0f_{5/2}, 1p_{3/2}, 1p_{1/2}, 0g_{9/2}$ proton and $0g_{7/2}, 1d_{5/2}, 1d_{3/2}, 2s_{1/2}$ neutron orbitals, that can be found in the Supplemental Material [75].

A. Spectroscopy of ^{100}Mo and ^{100}Ru

In Fig. 5, we compare the calculated low-energy spectra of ^{100}Mo and ^{100}Ru, as well as their experimental counterparts.

As can be seen, our H_{eff} provides a reasonable reproduction of ^{100}Mo low-lying states, despite the large number of valence nucleons involved in the diagonalization of the SM Hamiltonian. The larger discrepancy between observed and theoretical spectra occurs for the yrare $J^\pi = 0^+$ state, which exhibits experimentally a pronounced collective behavior. This is also testified by the $B(E2)$ strength between the $J^\pi = 0_2^+$ and $J^\pi = 2_1^+$ levels, that is reported in Table III. In fact, from the inspection of Table III, we see that there is a general agreement between theoretical and experimental values, but our calculation fails to reproduce the large $B(E2; 0_2^+ \to 2_1^+)$.

Once more, it is worth stressing that to calculate the $B(E2)$ strengths the effective proton/neutron charges have been derived from theory (see Sec. II B), without any empirical adjustment, and their values can be found in Table II.

Rearding the low-energy spectrum of ^{100}Ru, our calculation provides a satisfactory reproduction of the experiment, and this is also confirmed by the comparison of the theoretical $B(E2)$ strengths with the available data, as reported in Table IV.

We now proceed to examine the results of the calculation of quantities that are directly related to the double-β decay of ^{100}Mo. It is worth pointing out that, because of the proton and neutron model spaces, the effective GT$^+$ operator consists of one matrix element that corresponds to the $\pi 0g_{9/2} \to \nu 0g_{7/2}$ decay, whose calculated quenching factor is $q = 0.454$. Similarly, the only matrix element of the effective GT$^-$ operator $\nu 0g_{9/2} \to \pi 0g_{7/2}$ provides a quenching factor $q = 0.503$.

The reason for a non-Hermitian effective GT decay operator is threefold: the proton and neutron model spaces we have chosen are different, the proton-neutron symmetry is broken because the Coulomb interaction is included in the

TABLE II. Proton and neutron effective charges of the electric quadrupole operator $E2$.

$n_a l_a j_a\, n_b l_b j_b$	$\langle a\|\|e_p\|\|b\rangle$	$n_a l_a j_a\, n_b l_b j_b$	$\langle a\|\|e_n\|\|b\rangle$
$0f_{5/2}\,0f_{5/2}$	1.62	$0g_{7/2}\,0g_{7/2}$	1.00
$0f_{5/2}\,1p_{3/2}$	1.45	$0g_{7/2}\,1d_{5/2}$	0.73
$0f_{5/2}\,1p_{1/2}$	1.47	$0g_{7/2}\,1d_{3/2}$	0.70
$1p_{3/2}\,0f_{5/2}$	1.28	$1d_{5/2}\,0g_{7/2}$	0.68
$1p_{3/2}\,1p_{3/2}$	1.20	$1d_{5/2}\,1d_{5/2}$	0.47
$1p_{3/2}\,1p_{1/2}$	1.21	$1d_{5/2}\,1d_{3/2}$	0.48
$1p_{1/2}\,0f_{5/2}$	1.31	$1d_{5/2}\,2s_{1/2}$	0.43
$0g_{1/2}\,1p_{3/2}$	1.22	$1d_{3/2}\,0g_{7/2}$	0.66
$0g_{9/2}\,0g_{9/2}$	1.70	$1d_{3/2}\,1d_{5/2}$	0.48
		$1d_{3/2}\,1d_{3/2}$	0.55
		$1d_{3/2}\,2s_{1/2}$	0.50
		$2s_{1/2}\,1d_{5/2}$	0.43
		$2s_{1/2}\,1d_{3/2}$	0.50
		$0h_{11/2}\,0h_{11/2}$	0.79

perturbative expansion, and the procedure that has been followed to derive the effective operators is non-Hermitian [58].

In Table V we report the observed and calculated values of the $M^{2\nu}$'s for the $2\nu\beta\beta$ decay of ^{100}Mo from the $J^\pi = 0_1^+$ ground state (g.s.) to the ^{100}Ru $J^\pi = 0_1^+, 0_2^+$ states. For both decays the value of $M^{2\nu}$ obtained with the bare operator overestimates the experimental one by a factor of 3–4, but, employing the matrix elements of the effective GT$^+$ and GT$^-$ operators, we reach a result that is in a good agreement with the observed $M^{2\nu}$'s.

In Fig. 6, the calculated $\sum B(\mathrm{GT})$ for ^{100}Mo are shown as a function of the ^{100}Tc excitation energy, and compared with the data, reported with a red line [91]. The results obtained with the bare operator are drawn with a blue line, while those obtained employing the effective GT operator are plotted a black line.

It can be seen that the distribution obtained using the bare operator overestimates the observed one, but the quenching induced by the effective operator provides an underestimation of the values extracted from the experiment.

Here, recall that the "experimental" GT strengths obtained from charge-exchange reactions are not directly observed

TABLE III. Experimental and calculated $B(E2)$ strengths (in $e^2\mathrm{fm}^4$) for ^{100}Mo; data are taken from Ref. [89]. We report those for the observed states in Fig. 5.

$J_i \to J_f$	$B(E2)_{\mathrm{Expt}}$	$B(E2)_{\mathrm{Calc}}$
$2_1^+ \to 0_1^+$	1000 ± 100	820
$0_2^+ \to 2_1^+$	2500 ± 100	55
$2_2^+ \to 0_1^+$	17 ± 1	30
$2_2^+ \to 2_1^+$	1400 ± 140	800
$2_2^+ \to 0_2^+$	150 ± 20	540
$4_1^+ \to 2_1^+$	1900 ± 100	1200
$2_3^+ \to 2_1^+$	8 ± 2	15
$2_3^+ \to 0_2^+$	400 ± 100	340
$6_1^+ \to 4_1^+$	2500 ± 400	1240

TABLE IV. Experimental and calculated $B(E2)$ strengths (in $e^2\mathrm{fm}^4$) for ^{100}Ru; data are taken from Ref. [89]. We report those for the observed states in Fig. 5.

$J_i \to J_f$	$B(E2)_{\mathrm{Expt}}$	$B(E2)_{\mathrm{Calc}}$
$2_1^+ \to 0_1^+$	980 ± 10	640
$0_2^+ \to 2_1^+$	1000 ± 140	300
$4_1^+ \to 2_1^+$	1400 ± 100	980
$2_2^+ \to 2_1^+$	850 ± 170	570
$2_2^+ \to 0_1^+$	55 ± 10	50
$2_3^+ \to 4_1^+$	500 ± 140	90
$2_3^+ \to 0_2^+$	1000 ± 250	360

data. The GT strength can be extracted from the GT component of the cross section at zero degrees, following the standard approach in the distorted-wave Born approximation (DWBA):

$$\frac{d\sigma^{GT}(0^\circ)}{d\Omega} = \left(\frac{\mu}{\pi\hbar^2}\right)^2 \frac{k_f}{k_i} N_D^{\sigma\tau} |J_{\sigma\tau}|^2 B(\mathrm{GT}),$$

where $N_D^{\sigma\tau}$ is the distortion factor, $|J_{\sigma\tau}|$ is the volume integral of the effective NN interaction, k_i and k_f are the initial and final momenta, respectively, and μ is the reduced mass (see the formula and description in Refs. [92,93]). Then, the values of experimental GT strengths are somehow model dependent.

B. Neutrinoless double-β decay of ^{100}Mo

As introduced in Sect. II, our calculation of $M^{0\nu}$ accounts for the light-neutrino exchange mechanism, the total nuclear matrix element being expressed as in Eq. (19) and calculated according to Eqs. (13)–(15), (20), and (21), namely within the closure approximation.

The perturbative expansion of the $0\nu\beta\beta$ effective operator Θ_{eff} has been carried out including in the $\hat{\Theta}$ box diagrams up to the third order (see Sec. II) and a number of intermediate states which correspond to oscillator quanta up to $N_{\max} = 14$, since the results are substantially convergent from $N_{\max} = 12$ on (see Ref. [64]).

Regarding the expansion of Θ_{eff} as a function of the χ_n operators, we stop at $n = 2$ since χ_3 depends on the first, second, and third derivatives of $\hat{\Theta}_0$ and $\hat{\Theta}_{00}$, as well as on the first and second derivatives of the $\hat{Q}$ box [see Eq. (7)], so the χ_3 contribution may be estimated to be at least one order of magnitude smaller than the χ_2 one. Moreover, in Ref. [64] we have shown that the contributions from χ_1 are relevant, while those from χ_2 are almost negligible.

TABLE V. Experimental [90] and calculated $M^{2\nu}$'s (in MeV^{-1}) for ^{100}Mo $2\nu\beta\beta$ decay. The theoretical values are obtained employing both the bare (I) and effective (II) $2\nu\beta\beta$ operators.

^{100}Mo $\to$ ^{100}Ru decay branches	Experiment	I	II
$J^\pi = 0_1^+ \to J^\pi = 0_1^+$	0.224 ± 0.002	0.896	0.205
$J^\pi = 0_1^+ \to J^\pi = 0_2^+$	0.182 ± 0.006	0.479	0.109

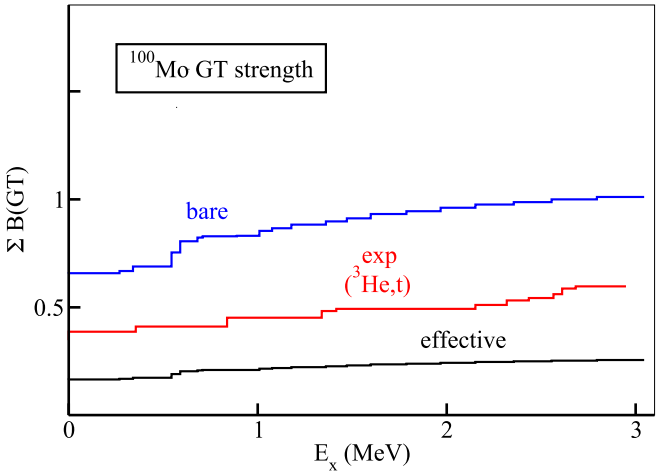

FIG. 6. Running sums of the ^{100}Mo $\sum B(\mathrm{GT})$ strengths as a function of the excitation energy E_x up to 3 MeV.

First, we focus on the results of the order-by-order convergence behavior by reporting in Figs. 7 and 8 the calculated values of $M^{0\nu}$, $M^{0\nu}_{\mathrm{GT}}$, $M^{0\nu}_{F}$, and $M^{0\nu}_{T}$ for the decay of the ^{100}Mo $J^\pi = 0^+_1$ state to the ^{100}Ru $J^\pi = 0^+_1, 0^+_2$ ones, respectively, from first order up to third order in perturbation theory. As an indicator of the quality of the perturbative behavior [94], we also report the values of their Padé approximant [2|1]. We also point out that the same scale has been adopted in both figures.

As in other decays we have studied in our previous work [64], the perturbative behavior is driven by the Gamow-Teller component, since the Fermi matrix element $M^{0\nu}_{\mathrm{F}}$ is weakly affected by the renormalization procedure, and $M^{0\nu}_{T}$ is almost negligible. We observe a perturbative pattern of the calculated $M^{0\nu}$ of ^{100}Mo that is better than the ones we have found for ^{48}Ge, ^{76}Ge, ^{82}Se, ^{130}Te, and ^{136}Xe $0\nu\beta\beta$ decays, which have been calculated within the same approach [64]. In fact, here the difference between second- and third-order results is about

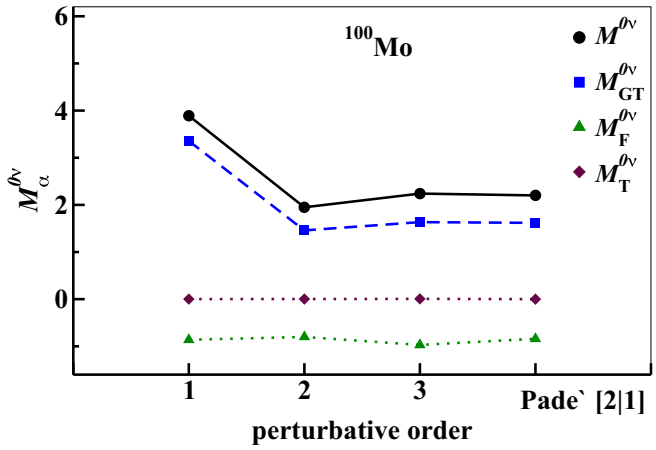

FIG. 7. $M^{0\nu}$ for the decay of the ^{100}Mo $J^\pi = 0^+_1$ state to the ^{100}Ru $J^\pi = 0^+_1$ one, as a function of the perturbative order. The green triangles correspond to $M^{0\nu}_{\mathrm{F}}$, the blue squares to $M^{0\nu}_{\mathrm{GT}}$, the magenta diamonds to $M^{0\nu}_{T}$, and the black dots to the full $M^{0\nu}$.

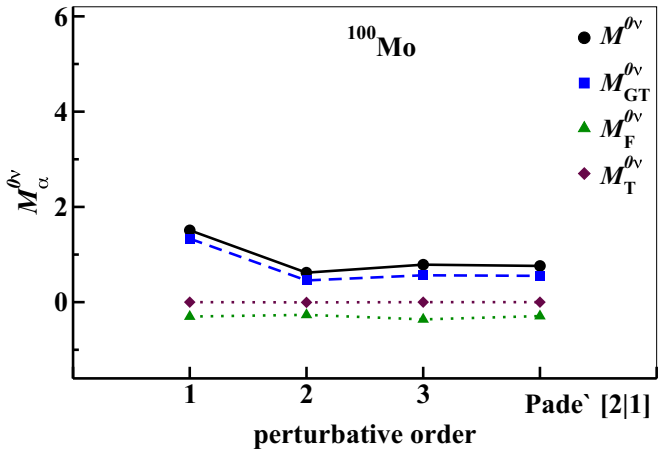

FIG. 8. Same as in Fig. 7, but for the decay of the ^{100}Mo $J^\pi = 0^+_1$ state to the ^{100}Ru $J^\pi = 0^+_2$ one.

13% and 21% for the decay of the ^{100}Mo $J^\pi = 0^+_1$ state to the ^{100}Ru $J^\pi = 0^+_1$ and $J^\pi = 0^+_2$ ones, respectively.

In Table VI the values of $M^{0\nu}$, which we have calculated by using both the bare operator—namely without considering either SRC or renormalizations due to the truncation of the model space—and Θ_{eff}, are reported, along with their Gamow-Teller, Fermi, and tensor components. Our results are also compared with those obtained employing other nuclear models, such as the interacting boson model with isospin restoration (IBM-2) [47], the energy density functional method including deformation and pairing fluctuations (EDF) [46], the beyond-mean-field covariant density functional theory (BMF-CDFT) [21], and the quasiparticle random-phase approximation with isospin symmetry restoration (pnQRPA) [51,52].

The SM results obtained with the bare $0\nu\beta\beta$ operator (I) can be better compared with other nuclear models, since in the latter no effective operator has been considered, and we see that our $M^{0\nu}$'s are close to those in Refs. [47,52], where the IBM-2 and pnQRPA models have been employed, respectively. The other calculations provide $M^{0\nu}$'s that are much

TABLE VI. Calculated values of $M^{0\nu}$ for the decay of the ^{100}Mo ground state to the yrast and yrare $J^\pi = 0^+$ states of ^{100}Ru.

	$M^{0\nu}_{\mathrm{GT}}$	$M^{0\nu}_{F}$	$M^{0\nu}_{T}$	$M^{0\nu}$
		$0^+_1 \to 0^+_1$		
Present work (I)	3.418	−0.878	0.002	3.962
Present work (II)	1.634	−0.970	0.007	2.240
IBM-2 [47]	3.73	−0.48	0.19	4.22
EDF [46]	5.361	−1.986		6.588
BMF-CDFT [21]				10.91
pnQRPA [51]	4.950	−2.367	−0.571	5.850
pnQRPA [52]	3.13	−1.03	−0.26	3.90
		$0^+_1 \to 0^+_2$		
Present work (I)	1.344	−0.308	0.001	1.535
Present work (II)	0.564	−0.361	0.001	0.788
IBM-2 [47]	0.99	−0.13	0.05	1.12

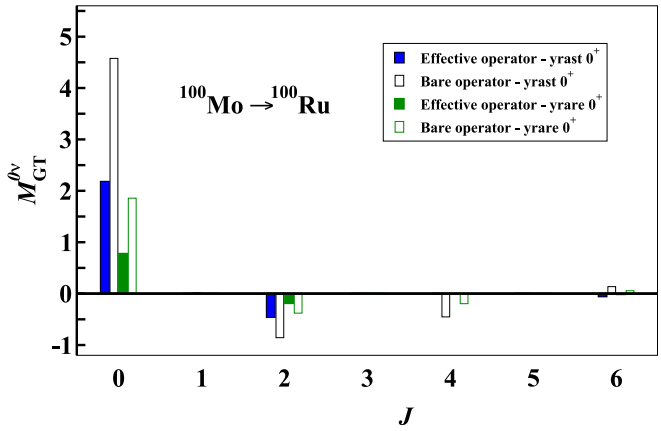

FIG. 9. Contributions from pairs of decaying neutrons with given J^π to $M^{0\nu}_{\rm GT}$ for ^{100}Mo $0\nu\beta\beta$ decay. The solid blue bars correspond to the results obtained with $\Theta_{\rm eff}$; those in crosshatched blue to the ones calculated with the bare operator.

larger than our result, and it is worth pointing out that different choices of the parameters for pnQRPA calculations may lead to a remarkable difference of the calculated $M^{0\nu}$'s [51,52].

The action of the effective operator $\Theta_{\rm eff}$ quenches the value of the two $M^{0\nu}$'s by a factor about $1/2$, whose effect is smaller than accounting for the quenching factor of the axial coupling constant g_A that comes out from the calculated effective GT$^\pm$ operator, which is about $q = 0.5$.

These considerations are related to the question of whether or not one should relate the derivation of the effective one-body GT operator [63] with the renormalization of the two-body GT component of the $0\nu\beta\beta$ operator. This issue has a considerable impact on the detectability of $0\nu\beta\beta$ process [95,96].

To complete our discussion about the $M^{0\nu}$'s, we show in Figs. 9 and 10 the results of the decomposition of $M^{0\nu}_{\rm GT}$ and $M^{0\nu}_F$, respectively, in terms of the contributions from the decaying pair of neutrons coupled to a given angular momentum and parity J^π, both for the decay to the ^{100}Ru ground (blue columns) and yrare $J^\pi = 0^+$ (green columns) states.

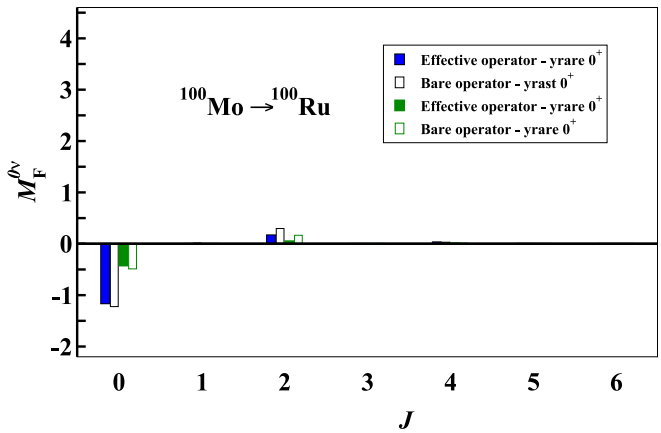

FIG. 10. Same as in Fig. 9, but for $M^{0\nu}_F$.

We report the contributions obtained by employing both the effective $0\nu\beta\beta$-decay operator $\Theta_{\rm eff}$ (filled columns) and the bare one (crosshatched columns).

The results of the decomposition of $M^{0\nu}_F$ confirm the irrelevance of the renormalization procedure, and exhibit the dominance of the $J^\pi = 0^+$ component.

Regarding $M^{0\nu}_{\rm GT}$, as should be expected, each J^π contribution calculated employing $\Theta_{\rm eff}$ is much smaller than the one obtained with the bare $0\nu\beta\beta$-decay operator. The main contributions, both employing effective and bare operators, correspond to the $J^\pi = 0^+, 2^+$ components, being opposite in sign, and a non-negligible role is played by the $J^\pi = 4^+$ component too.

IV. SUMMARY AND OUTLOOK

This work is the first attempt to calculate double-β decay of ^{100}Mo into ^{100}Ru by way of the nuclear shell model.

Our study consisted first in verifying the ability of the tools we have chosen, namely the model space and the shell-model effective Hamiltonian and decay operators, to reproduce the experimental spectroscopic properties of ^{100}Mo, Ru—excitation spectra and $B(E2)$ strengths that are related to the collective behavior of these systems—as well as the nuclear matrix elements $M^{2\nu}$ of the $2\nu\beta\beta$ decay and the GT strengths obtained from charge-exchange reactions. Then, after having tested and shown the degree of reliability of our wave functions, we calculated the nuclear matrix elements $M^{0\nu}$ of the $0\nu\beta\beta$ decay of the ^{100}Mo ground state to the yrast and yrare $J^\pi = 0^+$ states of ^{100}Ru.

An important feature of our work is that shell-model effective Hamiltonians and decay operators have been derived by way of many-body perturbation theory, starting from a high-precision realistic potential CD-Bonn [54]. Such an approach has been previously applied to study the ^{48}Ca $\to$ ^{48}Ti, ^{76}Ge $\to$ ^{76}Se, ^{82}Se $\to$ ^{82}Kr, ^{130}Te $\to$ ^{130}Xe, and ^{136}Xe $\to$ ^{136}Ba decays [62–64].

The comparison of our results with the available data seems to indicate that the realistic shell model can quantitatively describe most of the spectroscopy (low-lying excitation spectra, electromagnetic transition strengths) of ^{100}Mo, Ru and also their β-decay properties (nuclear matrix elements of $2\nu\beta\beta$ decay, GT strengths from charge-exchange reactions) without resorting to empirical adjustments of $H_{\rm eff}$, effective charges, or quenching the axial coupling constant. This should provide support to our approach for the prediction of the $M^{0\nu}$'s for the $0\nu\beta\beta$ decay of ^{100}Mo, within the light-neutrino-exchange channel, that is a conjugation of the action of shell-model wave functions, emerging from the diagonalization of $H_{\rm eff}$, and effective decay operators, which are constructed consistently with $H_{\rm eff}$.

We have also compared our results for the $0\nu\beta\beta$ decay of ^{100}Mo with those obtained employing other nuclear methods, leading to some relevant observations. To this end, we have considered the results we obtain employing both the bare $0\nu\beta\beta$ operator—namely without any sort of normalization—and the effective operator derived theoretically. The $M^{0\nu}$'s we calculate with the bare operator are important for a fair comparison with other nuclear models, since the latter do not

employ any effective operator which accounts for the truncation of the Hilbert space.

First, it can be noticed that our results with the bare operator are consistent with recent calculations performed with IBM-2 [47] and pnQRPA [52], whereas the results obtained within EDF [46] and BMF-CDFT [21] approaches, as well as pnQRPA calculations performed by Šimkovic *et al.* [51], provide larger values of $M^{0\nu}$'s.

Second, as in our previous study [64], the effect of the renormalization of the $0\nu\beta\beta$-decay operator, with respect to the truncation of the full Hilbert space to the shell-model one, is smaller than the one obtained for the $2\nu\beta\beta$-decay one.

These results may be a valuable asset for the community that is involved with the experimental detection of the ^{100}Mo $0\nu\beta\beta$ decay, since this is the first time a microscopic calculation has been performed of the $M^{0\nu}$'s of the ^{100}Mo ground-state decay to the two lowest-energy $J^{\pi} = 0^{+}$ states of ^{100}Ru.

Our future program to upgrade the study of nuclei with mass $A \approx 100$ which are candidates for $0\nu\beta\beta$ decay is twofold.

On one side, we plan to start from nuclear forces that have a firm link with QCD, namely we will construct effective shell-model Hamiltonians and decay operators from two- and three-body potentials derived within the framework of chiral perturbation theory [74,97,98].

This step will allow us

(a) to evaluate the dependence of the predictions for $M^{0\nu}$'s on the nuclear potential that is employed in a nuclear structure calculation;

(b) to benchmark our results with those obtained with *ab initio* calculations [13–15];

(c) to consider the contribution of the two-body meson-exchange corrections to the electroweak currents, originating from subnucleonic degrees of freedom, that can be consistently tackled by employing nuclear chiral potentials.

Alternatively, we are currently exploring the possibility of employing larger model spaces, that would account better for the low-energy collective behavior of nuclei with mass $A \approx 100$. This would provide major information about the connection between the calculated values of the $M^{0\nu}$'s and the dimension of the model space, and how theoretical effective decay operators can compensate and reduce this dependence.

These goals are computationally challenging, but we are confident that our current efforts may lead in the near future to a first set of preliminary results.

ACKNOWLEDGMENTS

We acknowledge a CINECA grant under the ISCRA initiative through the INFN-CINECA agreement, for the availability of high performance computing resources and support. We acknowledge PRACE for granting access to the Fenix Infrastructure resources, which are partially funded from the European Union's Horizon 2020 research and innovation program through the ICEI project under Grant Agreement No. 800858. G.D.G. acknowledges support by the funding program "VALERE" of Università degli Studi della Campania "Luigi Vanvitelli."

[1] Y. Fukuda, T. Hayakawa, E. Ichihara, K. Inoue, K. Ishihara, H. Ishino, Y. Itow, T. Kajita, J. Kameda, S. Kasuga *et al.* (Super-Kamiokande Collaboration), Phys. Rev. Lett. **81**, 1562 (1998).

[2] Q. R. Ahmad, R. C. Allen, T. C. Andersen, J. D. Anglin, G. Bühler, J. C. Barton, E. W. Beier, M. Bercovitch, J. Bigu, S. Biller *et al.* (SNO Collaboration), Phys. Rev. Lett. **87**, 071301 (2001).

[3] D. Falcone and F. Tramontano, Phys. Rev. D **64**, 077302 (2001).

[4] R. Mohapatra and A. Smirnov, Annu. Rev. Nucl. Part. Sci. **56**, 569 (2006).

[5] S. Dell'Oro, S. Marcocci, M. Viel, and F. Vissani, Adv. High Energy Phys. **2016**, 2162659 (2016).

[6] J. Kotila and F. Iachello, Phys. Rev. C **85**, 034316 (2012).

[7] J. Kotila and F. Iachello, Phys. Rev. C **87**, 024313 (2013).

[8] F. T. Avignone, S. R. Elliott, and J. Engel, Rev. Mod. Phys. **80**, 481 (2008).

[9] M. Tanabashi, K. Hagiwara, K. Hikasa, K. Nakamura, Y. Sumino, F. Takahashi, J. Tanaka, K. Agashe, G. Aielli, C. Amsler *et al.* (Particle Data Group), Phys. Rev. D **98**, 030001 (2018).

[10] S. Pastore, J. Carlson, V. Cirigliano, W. Dekens, E. Mereghetti, and R. B. Wiringa, Phys. Rev. C **97**, 014606 (2018).

[11] V. Cirigliano, W. Dekens, J. de Vries, M. L. Graesser, E. Mereghetti, S. Pastore, and U. van Kolck, Phys. Rev. Lett. **120**, 202001 (2018).

[12] V. Cirigliano, W. Dekens, J. de Vries, M. L. Graesser, E. Mereghetti, S. Pastore, M. Piarulli, U. van Kolck, and R. B. Wiringa, Phys. Rev. C **100**, 055504 (2019).

[13] J. M. Yao, B. Bally, J. Engel, R. Wirth, T. R. Rodríguez, and H. Hergert, Phys. Rev. Lett. **124**, 232501 (2020).

[14] S. Novario, P. Gysbers, J. Engel, G. Hagen, G. R. Jansen, T. D. Morris, P. Navrátil, T. Papenbrock, and S. Quaglioni, Phys. Rev. Lett. **126**, 182502 (2021).

[15] A. Belley, C. G. Payne, S. R. Stroberg, T. Miyagi, and J. D. Holt, Phys. Rev. Lett. **126**, 042502 (2021).

[16] J. Barea, J. Kotila, and F. Iachello, Phys. Rev. C **87**, 014315 (2013).

[17] J. Terasaki, Phys. Rev. C **91**, 034318 (2015).

[18] D.-L. Fang, A. Faessler, and F. Šimkovic, Phys. Rev. C **97**, 045503 (2018).

[19] T. R. Rodríguez and G. Martínez-Pinedo, Phys. Rev. Lett. **105**, 252503 (2010).

[20] T. R. Rodríguez and M.-P. Gabriel, Phys. Lett. B **719**, 174 (2013).

[21] J. M. Yao, L. S. Song, K. Hagino, P. Ring, and J. Meng, Phys. Rev. C **91**, 024316 (2015).

[22] L. S. Song, J. M. Yao, P. Ring, and J. Meng, Phys. Rev. C **95**, 024305 (2017).

[23] C. F. Jiao, J. Engel, and J. D. Holt, Phys. Rev. C **96**, 054310 (2017).

[24] C. F. Jiao, M. Horoi, and A. Neacsu, Phys. Rev. C **98**, 064324 (2018).
[25] R. A. Sen'kov and M. Horoi, Phys. Rev. C **88**, 064312 (2013).
[26] J. D. Holt and J. Engel, Phys. Rev. C **87**, 064315 (2013).
[27] R. A. Sen'kov, M. Horoi, and B. A. Brown, Phys. Rev. C **89**, 054304 (2014).
[28] A. Neacsu and M. Horoi, Phys. Rev. C **91**, 024309 (2015).
[29] J. Menéndez, J. Phys. G **45**, 014003 (2017).
[30] L. Coraggio, N. Itaco, G. De Gregorio, A. Gargano, R. Mancino, and S. Pastore, Universe **6**, 233 (2020).
[31] M. Wang, G. Audi, F. G. Kondev, W. J. Huang, S. Naimi, and X. Xing, Chin. Phys. C **41**, 030003 (2017).
[32] V. Alenkov, H. W. Bae, J. Beyer, R. S. Boiko, K. Boonin, O. Buzanov, N. Chanthima, M. K. Cheoun, D. M. Chernyak, J. S. Choe *et al.*, Eur. Phys. J. C **79**, 791 (2019).
[33] H. Bhang, R. S. Boiko, D. M. Chernyak, J. H. Choi, S. Choi, F. A. Danevich, K. V. Efendiev, C. Enss, A. Fleischmann, A. M. Gangapshev *et al.*, J. Phys.: Conf. Ser. **375**, 042023 (2012).
[34] R. Arnold, C. Augier, J. Baker, A. Barabash, M. Bongrand, G. Broudin, V. Brudanin, A. Caffrey, V. Egorov, A. Etienvre *et al.*, Nucl. Phys. A **781**, 209 (2007).
[35] E. Armengaud, C. Augier, A. S. Barabash, F. Bellini, G. Benato, A. Benoît, M. Beretta, L. Bergé, J. Billard, Y. A. Borovlev *et al.* (CUPID-Mo Collaboration), Eur. Phys. J. C **80**, 674 (2020).
[36] E. Armengaud, C. Augier, A. S. Barabash, F. Bellini, G. Benato, A. Benoît, M. Beretta, L. Bergé, J. Billard, Y. A. Borovlev *et al.* (CUPID-Mo Collaboration), Phys. Rev. Lett. **126**, 181802 (2021).
[37] CUPID Interest Group, arXiv:1907.09376.
[38] E. Cheifetz, R. C. Jared, S. G. Thompson, and J. B. Wilhelmy, Phys. Rev. Lett. **25**, 38 (1970).
[39] P. von Brentano, V. Werner, R. F. Casten, C. Scholl, E. A. McCutchan, R. Krücken, and J. Jolie, Phys. Rev. Lett. **93**, 152502 (2004).
[40] P. Cejnar and J. Jolie, Phys. Rev. C **69**, 011301(R) (2004).
[41] C. L. Zhang, G. H. Bhat, W. Nazarewicz, J. A. Sheikh, and Y. Shi, Phys. Rev. C **92**, 034307 (2015).
[42] J. Xiang, J. M. Yao, Y. Fu, Z. H. Wang, Z. P. Li, and W. H. Long, Phys. Rev. C **93**, 054324 (2016).
[43] H. Abusara, S. Ahmad, and S. Othman, Phys. Rev. C **95**, 054302 (2017).
[44] I. P. Johnstone and I. S. Towner, Eur. Phys. J. A **3**, 237 (1998).
[45] C. Özen and D. J. Dean, Phys. Rev. C **73**, 014302 (2006).
[46] N. L. Vaquero, T. R. Rodríguez, and J. L. Egido, Phys. Rev. Lett. **111**, 142501 (2013).
[47] J. Barea, J. Kotila, and F. Iachello, Phys. Rev. C **91**, 034304 (2015).
[48] T. Tomoda, Rep. Prog. Phys. **54**, 53 (1991).
[49] G. Pantis, F. Šimkovic, J. D. Vergados, and A. Faessler, Phys. Rev. C **53**, 695 (1996).
[50] K. Chaturvedi, B. M. Dixit, P. K. Rath, and P. K. Raina, Phys. Rev. C **67**, 064317 (2003).
[51] F. Šimkovic, V. Rodin, A. Faessler, and P. Vogel, Phys. Rev. C **87**, 045501 (2013).
[52] J. Hyvärinen and J. Suhonen, Phys. Rev. C **91**, 024613 (2015).
[53] L. Coraggio, A. Covello, A. Gargano, N. Itaco, and T. T. S. Kuo, Prog. Part. Nucl. Phys. **62**, 135 (2009).
[54] R. Machleidt, Phys. Rev. C **63**, 024001 (2001).
[55] S. Bogner, T. T. S. Kuo, L. Coraggio, A. Covello, and N. Itaco, Phys. Rev. C **65**, 051301(R) (2002).
[56] T. T. S. Kuo, F. Krmpotić, K. Suzuki, and R. Okamoto, Nucl. Phys. A **582**, 205 (1995).
[57] M. Hjorth-Jensen, T. T. S. Kuo, and E. Osnes, Phys. Rep. **261**, 125 (1995).
[58] K. Suzuki and R. Okamoto, Prog. Theor. Phys. **93**, 905 (1995).
[59] L. Coraggio, A. Covello, A. Gargano, N. Itaco, and T. T. S. Kuo, Ann. Phys. (NY) **327**, 2125 (2012).
[60] P. J. Ellis and E. Osnes, Rev. Mod. Phys. **49**, 777 (1977).
[61] L. Coraggio and N. Itaco, Front. Phys. **8**, 345 (2020).
[62] L. Coraggio, L. De Angelis, T. Fukui, A. Gargano, and N. Itaco, Phys. Rev. C **95**, 064324 (2017).
[63] L. Coraggio, L. De Angelis, T. Fukui, A. Gargano, N. Itaco, and F. Nowacki, Phys. Rev. C **100**, 014316 (2019).
[64] L. Coraggio, A. Gargano, N. Itaco, R. Mancino, and F. Nowacki, Phys. Rev. C **101**, 044315 (2020).
[65] K. Sieja, F. Nowacki, K. Langanke, and G. Martínez-Pinedo, Phys. Rev. C **79**, 064310 (2009).
[66] L. Coraggio, A. Gargano, and N. Itaco, Phys. Rev. C **93**, 064328 (2016).
[67] L. Coraggio, A. Covello, A. Gargano, N. Itaco, and T. T. S. Kuo, Phys. Rev. C **91**, 041301(R) (2015).
[68] L. Coraggio, N. Itaco, and R. Mancino, J. Phys.: Conf. Ser. **1643**, 012124 (2020).
[69] T. T. S. Kuo and E. Osnes, *Folded-Diagram Theory of the Effective Interaction in Nuclei, Atoms and Molecules*, Lecture Notes in Physics Vol. 364 (Springer-Verlag, Berlin, 1990).
[70] E. M. Krenciglowa and T. T. S. Kuo, Nucl. Phys. A **235**, 171 (1974).
[71] K. Suzuki and S. Y. Lee, Prog. Theor. Phys. **64**, 2091 (1980).
[72] K. Suzuki, R. Okamoto, H. Kumagai, and S. Fujii, Phys. Rev. C **83**, 024304 (2011).
[73] E. Caurier, G. Martínez-Pinedo, F. Nowacki, A. Poves, and A. P. Zuker, Rev. Mod. Phys. **77**, 427 (2005).
[74] L. Coraggio, G. De Gregorio, A. Gargano, N. Itaco, T. Fukui, Y. Z. Ma, and F. R. Xu, Phys. Rev. C **102**, 054326 (2020).
[75] See Supplemental Material at http://link.aps.org/supplemental/10.1103/PhysRevC.105.034312 for the list of two-body matrix elements of the shell-model Hamiltonian H_{eff}, derived for 14 and 8 valence protons and neutrons, respectively, namely for ^{100}Mo.
[76] H. A. Mavromatis, L. Zamick, and G. E. Brown, Nucl. Phys. A **80**, 545 (1966).
[77] H. A. Mavromatis and L. Zamick, Nucl. Phys. A **104**, 17 (1967).
[78] P. Federman and L. Zamick, Phys. Rev. **177**, 1534 (1969).
[79] I. S. Towner and K. F. C. Khanna, Nucl. Phys. A **399**, 334 (1983).
[80] I. S. Towner, Phys. Rep. **155**, 263 (1987).
[81] L. Coraggio, L. De Angelis, T. Fukui, A. Gargano, and N. Itaco, J. Phys.: Conf. Ser. **1056**, 012012 (2018).
[82] W. C. Haxton and G. J. Stephenson, Jr., Prog. Part. Nucl. Phys. **12**, 409 (1984).
[83] S. R. Elliott and V. Petr, Annu. Rev. Nucl. Part. Sci. **52**, 115 (2002).
[84] J. Engel and J. Menéndez, Rep. Prog. Phys. **80**, 046301 (2017).
[85] F. Šimkovic, A. Faessler, V. Rodin, P. Vogel, and J. Engel, Phys. Rev. C **77**, 045503 (2008).
[86] H. A. Bethe, Annu. Rev. Nucl. Sci. **21**, 93 (1971).
[87] M. Kortelainen, O. Civitarese, J. Suhonen, and J. Toivanen, Phys. Lett. B **647**, 128 (2007).

[88] J. Menéndez, A. Poves, E. Caurier, and F. Nowacki, Nucl. Phys. A **818**, 139 (2009).
[89] Data extracted using the NNDC On-line Data Service from the ENSDF database, file revised as of March 13, 2021, https://www.nndc.bnl.gov/ensdf.
[90] A. Barabash, Universe **6**, 159 (2020).
[91] J. H. Thies, T. Adachi, M. Dozono, H. Ejiri, D. Frekers, H. Fujita, Y. Fujita, M. Fujiwara, E. W. Grewe, K. Hatanaka, P. Heinrichs, D. Ishikawa, N. T. Khai, A. Lennarz, H. Matsubara, H. Okamura, Y. Y. Oo, P. Puppe, T. Ruhe, K. Suda, A. Tamii, H. P. Yoshida, and R. G. T. Zegers, Phys. Rev. C **86**, 044309 (2012).
[92] P. Puppe, A. Lennarz, T. Adachi, H. Akimune, H. Ejiri, D. Frekers, H. Fujita, Y. Fujita, M. Fujiwara, E. Ganioglu, E. W. Grewe, K. Hatanaka, R. Hodak, C. Iwamoto, N. T. Khai, A. Okamoto, H. Okamura, P. P. Povinec, G. Susoy, T. Suzuki, A. Tamii, J. H. Thies, and M. Yosoi, Phys. Rev. C **86**, 044603 (2012).
[93] D. Frekers, P. Puppe, J. H. Thies, and H. Ejiri, Nucl. Phys. A **916**, 219 (2013).
[94] G. A. Baker and J. L. Gammel, *The Padé Approximant in Theoretical Physics*, Mathematics in Science and Engineering Vol. 71 (Academic, New York, 1970).
[95] J. Suhonen, Phys. Rev. C **96**, 055501 (2017).
[96] J. T. Suhonen, Front. Phys. **5**, 55 (2017).
[97] T. Fukui, L. De Angelis, Y. Z. Ma, L. Coraggio, A. Gargano, N. Itaco, and F. R. Xu, Phys. Rev. C **98**, 044305 (2018).
[98] Y. Z. Ma, L. Coraggio, L. De Angelis, T. Fukui, A. Gargano, N. Itaco, and F. R. Xu, Phys. Rev. C **100**, 034324 (2019).